energies

MDPI

Article

Rotor Time Constant Identification Method for Induction Motors Based on an Improved Stator-Flux Model

Han He and Yun Zhao *

School of Electrical and Electronic Engineering, Hubei University of Technology, Wuhan 430068, China; 102410317@hbut.edu.cn

* Correspondence: 20141051@hbut.edu.cn; Tel.: +86-13871363285

Abstract

In induction motor drive systems employing indirect field-oriented control (IFOC), variations in the rotor time constant lead to inaccurate estimation of the rotor field phase, thereby preventing accurate decoupling of torque and flux. To solve this problem, this paper designs an online rotor time constant identification scheme based on an improved stator-flux model. Considering that the stator-flux model is susceptible to DC offset, a stator-flux observer with DC-offset compensation is designed. Based on the improved stator-flux model, a rotor-flux voltage model is established as the reference model of the model reference adaptive system (MRAS), while the rotor-flux current model is adopted as the adjustable model. The corresponding adaptation law is derived based on Popov's hyperstability theory to ensure the stability of the identification system. Simulation results show that the proposed observer reduces the relative flux estimation root-mean-square error from 37.38% to 2.05% in the DC-offset test. In the parameter identification test, the estimated inverse rotor time constant enters a ±2% error band in approximately 0.43 s and achieves a relative root-mean-square error of 0.51% over the interval from 1.5 to 2 s.

Keywords: induction motor; rotor time constant; stator flux; model reference adaptive system

1. Introduction

Induction motor drive systems employing indirect field-oriented control have been extensively applied to industrial applications, including machine tool spindle drives, electric vehicles, and rail transit because of their good dynamic performance and ease of implementation [1–3]. Recent studies have examined induction motor drives from the perspectives of efficiency, control, and transient operation. Azab reviewed developments in high-efficiency induction motor drives, including motor technologies, power converters, and control strategies [4]. Konuhova investigated induction motor responses to voltage sags and subsequent re-acceleration, highlighting the effects of supply disturbances on motor dynamics [5]. Regarding parameter-dependent control, Tang et al. reviewed identification methods for inverter-fed induction motors and discussed parameter variations associated with temperature, skin effect, and magnetic saturation [6]. In rotor flux-oriented control, accurate rotor-flux orientation is strongly influenced by the rotor time constant. However, during practical motor operation, the rotor time constant may vary significantly as a result of temperature changes and magnetic saturation [7–9]. If the controller uses an outdated rotor time constant, the rotor-flux phase observation error will

Academic Editor: Alessandro Niccolai

Received: 18 September 2026
Revised: 28 October 2026
Accepted: 2 November 2026
Published: 4 November 2026

Copyright: © 2026 by the authors. Licensee MDPI, Basel, Switzerland. This article is an open access article distributed under the terms and conditions of the Creative Commons Attribution (CC BY) license.

increase, preventing precise independent regulation of induction motor torque and flux, and consequently reducing its torque output capability and slowing the dynamic response [10]. To address this issue, various rotor time constant identification schemes have been proposed, including approaches based on sliding mode observers [11], model reference adaptive system methods [12], and extended Kalman filter methods [13]. Among these, MRAS has received considerable research attention owing to its simple structure and ease of implementation. A typical MRAS framework incorporates three essential elements, namely an adjustable model, a reference model, and an adaptation law. A reactive-power-based rotor time constant identification scheme is presented in [14]; however, this approach imposes relatively high requirements on the design of the adjustable model. Reference [15] constructs an identification system using the dot product of the stator current and rotor flux, which effectively suppresses the influence of the dead-time effect. However, this method relies on accurate rotor-flux information, and the pure integrator in conventional flux observation introduces a DC-offset problem. Zhong et al. [16] developed a ROGI-PNSS flux observer for PMSM sensorless control, incorporating DC-offset compensation and positive- and negative-sequence separation to suppress DC offsets and negative-sequence fundamental disturbances. The present study focuses on the flux reference model used for rotor time constant identification in induction motor drives. Feedback compensation is constructed from the steady-state relationship between the stator back electromotive force and flux linkage, and the resulting flux estimate is incorporated into an MRAS identification scheme.

To address integrator drift in the flux reference model, this paper develops a stator-flux observer with feedback compensation based on the steady-state relationship between the stator back electromotive force and flux linkage. The observer suppresses the accumulation of input offsets while preserving the ideal integrator response at the synchronous frequency under steady-state conditions. The resulting stator-flux estimate is used to construct the rotor-flux reference model for MRAS-based online rotor time constant identification. An adaptation law is derived using Popov hyperstability theory under the stated assumptions. Simulation comparisons assess the influence of the flux observer on flux estimation accuracy and rotor time constant identification performance.

2. Influence of Rotor Time Constant on IFOC

The fundamental principle of IFOC is to orient the d-axis of the synchronously rotating reference frame along the rotor-flux vector, enabling decoupled control of the induction motor flux and torque. To realize the IFOC of the induction motor, the key is to obtain the rotor field phase angle θ_e. The rotor field phase angle is indirectly determined by integrating the sum of the rotor electrical angular frequency and the slip angular frequency. This phase angle θ_e can be written as:

$$\begin{cases} \omega_{sl} = \dfrac{1}{T_r}\dfrac{i_{sq}}{i_{sd}}, T_r = \dfrac{L_r}{R_r} \\ \theta_e = \theta_r + \theta_{sl} = \int \left(\omega_r + \omega_{sl}\right) dt = \int \omega_e dt \end{cases} \tag{1}$$

In the above equation, ω_{sl}, ω_r and ω_e are the slip electrical angular frequency, the rotor electrical angular frequency, and the synchronous electrical angular velocity, respectively; i_{sd} and i_{sq} are the d-axis and q-axis components of the stator current, respectively; T_r, L_r, and R_r are the rotor time constant, rotor inductance, and rotor resistance, respectively; and θ_e, θ_r and θ_{sl} are the rotor field phase angle, the rotor position angle, and the slip angle, respectively. For the convenience of analysis and illustration, the following convention is adopted: $\hat{X}$ denotes the observed value, and X denotes the actual value.

https://doi.org/10.3390/en19215289

From Equation (1), it can be seen that the phase angle of the rotor field is determined by the slip angular frequency and the rotor angular frequency. Usually, the rotor position is detected using an encoder, and it can be considered that the rotor position angle θ_r has essentially no deviation. Therefore, the accuracy of observing the rotor field phase angle mainly depends on the calculation of the slip angle θ_{sl}.

According to Equation (1), if $\hat{T}_r = T_r$, then the observed value of the slip angular frequency equals the actual value, and $\hat{\theta}_e = \theta_e$; in this case, the observed rotor field position coincides with the actual position, and the field orientation is accurate. If $\hat{T}_r > T_r$, then $\hat{\omega}_{sl} < \omega_{sl}$, and therefore, $\hat{\theta}_e < \theta_e$; in this case, the observed rotor field position lags behind the actual position. If $\hat{T}_r < T_r$, then $\hat{\omega}_{sl} > \omega_{sl}$, and therefore, $\hat{\theta}_e > \theta_e$; in this case, the observed rotor field position leads ahead of the actual position. A schematic diagram of the rotor field phase observation deviation is shown in Figure 1.

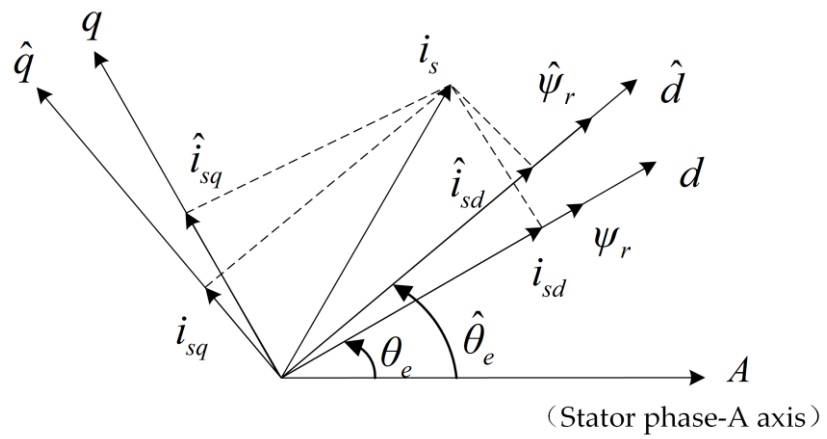


Figure 1. Rotor-flux phase estimation error.

As shown in Figure 1, when the rotor time constant changes, the observed rotor field position deviates from the actual position; at this time, $\hat{i}_{sd} \neq i_{sd}$, $\hat{i}_{sq} \neq i_{sq}$, and $\hat{\psi}_r \neq \psi_r$. The orientation error will cause the excitation component and torque component of the stator current to become coupled, making it impossible to control the flux and torque independently, and thus preventing accurate control of the induction motor.

Therefore, it is necessary to perform online identification of the rotor time constant of the induction motor.

3. Design of an Improved Stator-Flux Observer

Using the stationary α-β reference frame, the voltage equations of the induction motor can be written as:

$$\begin{cases} u_{s\alpha} = R_s i_{s\alpha} + p\psi_{s\alpha} \\ u_{s\beta} = R_s i_{s\beta} + p\psi_{s\beta} \\ u_{r\alpha} = R_r i_{r\alpha} + p\psi_{r\alpha} + \omega_r \psi_{r\beta} \\ u_{r\beta} = R_r i_{r\beta} + p\psi_{r\beta} - \omega_r \psi_{r\alpha} \end{cases} \quad (2)$$

In Equation (2), $\psi_{s\alpha}$ and $\psi_{s\beta}$ denote the α- and β-axis components of the stator-flux linkage; $\psi_{r\alpha}$ and $\psi_{r\beta}$ represent the corresponding rotor-flux linkage components; $u_{s\alpha}$ and $u_{s\beta}$ denote the α- and β-axis components of the stator voltage; $u_{r\alpha}$ and $u_{r\beta}$ represent the corresponding rotor voltage components; $i_{s\alpha}$ and $i_{s\beta}$ denote the α- and β-axis components of the stator current; $i_{r\alpha}$ and $i_{r\beta}$ represent the corresponding rotor

current components; R_s denotes the stator resistance; and p denotes the differential operator;

The flux linkage equations of the stator and rotor can be written as:

$$\begin{cases} \psi_{s\alpha} = L_s i_{s\alpha} + L_m i_{r\alpha} \\ \psi_{s\beta} = L_s i_{s\beta} + L_m i_{r\beta} \\ \psi_{r\alpha} = L_m i_{s\alpha} + L_r i_{r\alpha} \\ \psi_{r\beta} = L_m i_{s\beta} + L_r i_{r\beta} \end{cases} \tag{3}$$

In Equation (3), L_s denotes the stator inductance, whereas L_m represents the mutual inductance.

The electromagnetic torque equation can be written as:

$$T_e = n_p L_m \left(i_{s\beta} i_{r\alpha} - i_{s\alpha} i_{r\beta} \right) \tag{4}$$

In Equation (4), T_e denotes the electromagnetic torque, while n_p represents the number of pole pairs.

According to Equation (2), the stator-flux linkage in the induction motor can be written as:

$$\begin{cases} \psi_{s\alpha} = \int \left(u_{s\alpha} - R_s i_{s\alpha} \right) dt = \int e_{sa} dt \\ \psi_{s\beta} = \int \left(u_{s\beta} - R_s i_{s\beta} \right) dt = \int e_{s\beta} dt \end{cases} \tag{5}$$

According to Equation (3), the rotor-flux linkage of the induction motor can be written as:

$$\begin{cases} \psi_{r\alpha} = \dfrac{L_r}{L_m} \left(\psi_{s\alpha} - \sigma L_s i_{s\alpha} \right) \\ \psi_{r\beta} = \dfrac{L_r}{L_m} \left(\psi_{s\beta} - \sigma L_s i_{s\beta} \right) \end{cases} \tag{6}$$

In Equation (6), $\sigma = 1 - \dfrac{L_m^2}{L_s L_r}$ denotes the leakage coefficient.

Under steady-state conditions, the stator back electromotive force and the stator-flux linkage described by Equation (5) satisfy the following relationship:

$$e_s = j\omega_e \psi_s \tag{7}$$

In the above equation, e_s denotes the stator back electromotive force, and ψ_s represents the stator-flux linkage.

When DC components are present in the input voltage and current signals, Equation (5) can be expressed as:

$$\psi_s = \int \left(e_s + \Delta d \right) dt \tag{8}$$

In Equation (8), Δd denotes the total DC component. From the analysis of Equation (8), it can be seen that when the input electrical signals include DC components, these components are continuously integrated, causing the calculated stator-flux linkage to deviate from its true value.

The motivation for introducing feedback compensation is to prevent a constant input offset from accumulating indefinitely in the pure integrator while preserving the required integration response at the synchronous frequency. Under sinusoidal steady-state conditions, the stator back electromotive force and flux linkage satisfy Equation (7). A deviation

from this relationship is used to construct a feedback correction signal, denoted as Δd_s, which is expressed as:

$$\Delta d_s = |\omega_e|\psi_s - \frac{\mathrm{sgn}(\omega_e)e_s}{j} \tag{9}$$

Equation (9) is written in a form valid for both directions of rotation: the magnitude and the sign of the synchronous angular frequency are treated separately so that the compensation loop keeps a sign-definite gain when the motor reverses, and so that no division by ω_e is required near standstill.

Under ideal sinusoidal steady-state conditions and with accurate flux information, when there is no DC offset, $\Delta d_s = 0$, and when a DC offset exists, $\Delta d_s \neq 0$. During transients, however, this signal may also reflect deviations from the steady-state relationship in Equation (7), rather than DC offsets alone. After obtaining this signal, the DC offset of the integrator is compensated by means of a negative feedback signal with compensation feedback gain K_λ, and this feedback signal is fed to the input of the integrator. Therefore, the improved stator-flux mathematical model can be expressed as:

$$\psi_s^v = \frac{e_s - K_\lambda \Delta d_s}{s} \tag{10}$$

Considering the forward and reverse operating conditions of the induction motor, the configuration of the improved flux observer is illustrated in Figure 2.

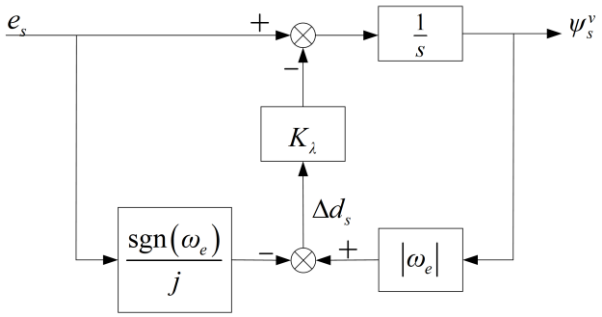


Figure 2. Improved stator-flux observer.

From Figure 2, the transfer function for the stator-flux observer can be written as:

$$G_e(s) = \frac{\psi_s^v}{e_s} = \frac{1 + \frac{K_\lambda}{j}\mathrm{sgn}(\omega_e)}{s + K_\lambda|\omega_e|} \tag{11}$$

In the steady state, Equation (11) can be simplified as:

$$G_e(s)\big|_{s=j\omega_e} = \frac{1}{j\omega_e} \tag{12}$$

Although Equation (12) shows that the observer preserves the ideal integrator response at the synchronous frequency under steady-state conditions, its DC gain is nonzero. For a fixed nonzero synchronous electrical angular frequency and a positive compensation gain, the DC gain is $G_e(0) = \frac{1 - jK_\lambda \,\mathrm{sgn}(\omega_e)}{K_\lambda |\,\omega_e\,|}$. Consequently, a constant input offset produces a finite steady-state flux error rather than the continuously increasing error associated with a pure integrator. The proposed observer therefore suppresses integrator drift but does not completely eliminate the offset-induced flux error.

From Equation (12), it can be seen that, under steady-state conditions, the frequency response of the improved stator-flux observer is equivalent to that of an integrator, so it is capable of observing the stator-flux linkage of the induction motor. In addition, from Equation (11), the expressions for the α - and β -axis components of the improved stator-flux linkage can be further obtained as:

$$\begin{cases} \psi_{s\alpha}^{v} = \dfrac{(u_{s\alpha} - R_s i_{s\alpha}) + K_\lambda \operatorname{sgn}(\omega_e)(u_{s\beta} - R_s i_{s\beta})}{s + K_\lambda |\omega_e|} \\ \psi_{s\beta}^{v} = \dfrac{(u_{s\beta} - R_s i_{s\beta}) - K_\lambda \operatorname{sgn}(\omega_e)(u_{s\alpha} - R_s i_{s\alpha})}{s + K_\lambda |\omega_e|} \end{cases} \tag{13}$$

Figure 3 shows the magnitude-frequency and phase-frequency characteristics of $G_e(s)$ when $\omega_e = 628$ rad/s and K_λ is set to 0.01, 1, and 10, respectively. Figure 4 shows the magnitude-frequency and phase-frequency characteristics of $G_e(s)$ when $K_\lambda = 10$ is given and ω_e is set to 31.4, 314, and 628 rad/s, respectively. It can be seen from Figure 3 that increasing K_λ results in a wider observer bandwidth and a faster dynamic response; however, in the high-frequency range, the observer becomes more sensitive to measurement noise. It can be seen from Figure 4 that as ω_e increases, the suppression effect of the observer on DC disturbances becomes more pronounced. Therefore, in this paper, K_λ is designed in the following form:

$$K_\lambda = \begin{cases} C, |\omega_e| < \omega_c \\ \dfrac{\omega_c}{|\omega_e|}, |\omega_e| \geq \omega_c \end{cases} \tag{14}$$

In Equation (14), C is the critical integral gain coefficient, generally taken as 1–10, and ω_c is the cutoff frequency, generally selected as 5–20% of the motor rated frequency.

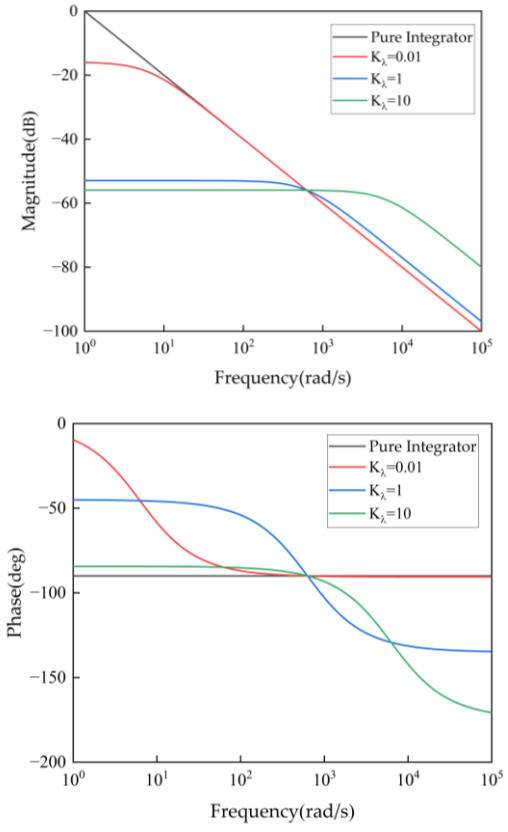


Figure 3. Bode diagrams under different values of K_λ.

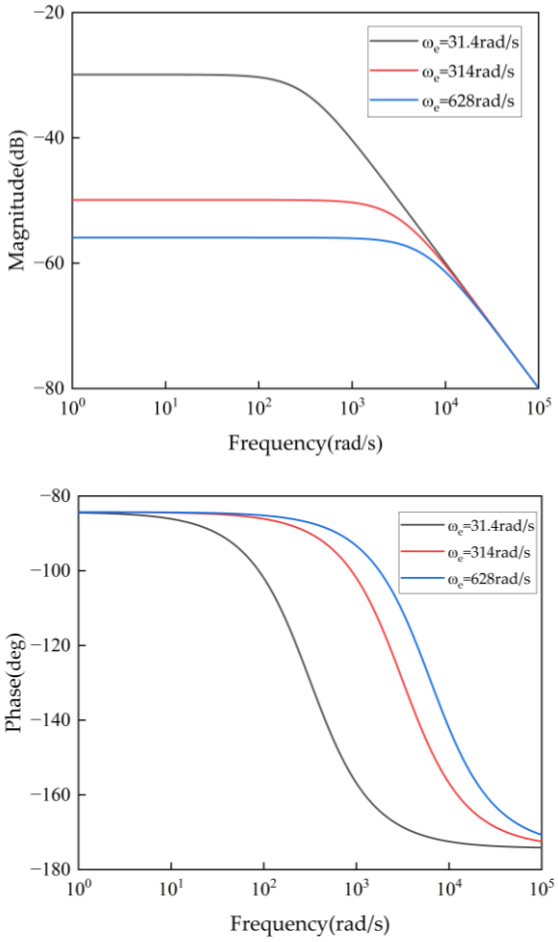


Figure 4. Bode diagrams under different values of ω_e.

4. MRAS Identification Method

4.1. Basic Principle

The structure of a model reference adaptive system generally includes an adjustable model, a reference model, and an adaptation mechanism [17–19]. Among them, the reference model does not contain the parameters to be identified, and its output is regarded as the ideal response; the adjustable model contains the parameters to be identified, and its output is affected by these parameters. The error between the outputs of the reference and adjustable models serves as the input to the adaptation mechanism, which then adjusts the identified parameters according to the adaptation law. The adaptation mechanism adjusts the estimated parameter to reduce the flux error between the reference and adjustable models. Convergence of this error to zero does not, by itself, guarantee convergence of the estimated parameter to its true value. Parameter convergence additionally requires an accurate reference model, sufficiently informative excitation, and identifiable operating conditions.

In this work, the improved rotor-flux voltage model is employed as the MRAS reference model, while the rotor-flux current model is adopted as the adjustable model. Since Popov hyperstability theory can guarantee system stability and convergence during the parameter identification process, this paper uses Popov hyperstability theory as the theoretical basis to design the adaptation law.

4.2. Design of the Adaptation Law

The conventional rotor-flux reference model is obtained by substituting Equation (5) into Equation (6). According to the analysis in Section 3, the DC-offset problem will lead to inaccurate observation of the stator-flux linkage, which consequently affects the accuracy of the rotor-flux reference model. To enhance the accuracy of the rotor-flux reference model, this paper constructs the reference model for rotor flux using the improved stator-flux linkage. This rotor-flux reference model can be expressed as:

$$\begin{cases} \psi_{r\alpha} = \dfrac{L_r}{L_m}\left(\psi^{v}_{s\alpha} - \sigma L_s i_{s\alpha}\right) \\ \psi_{r\beta} = \dfrac{L_r}{L_m}\left(\psi^{v}_{s\beta} - \sigma L_s i_{s\beta}\right) \end{cases} \tag{15}$$

The rotor-flux adjustable model can be expressed as:

$$p\begin{bmatrix} \psi_{r\alpha} \\ \psi_{r\beta} \end{bmatrix} = \begin{bmatrix} -\tau_r & -\omega_r \\ \omega_r & -\tau_r \end{bmatrix}\begin{bmatrix} \psi_{r\alpha} \\ \psi_{r\beta} \end{bmatrix} + L_m\tau_r\begin{bmatrix} i_{s\alpha} \\ i_{s\beta} \end{bmatrix} \tag{16}$$

In Equation (16), $\tau_r = \dfrac{1}{T_r}$ is the reciprocal of the rotor time constant. When T_r in the controller is consistent with its true value, the calculated flux linkage results of the two models are identical.

On this basis, replacing the actual value in Equation (16) with the estimated value $\hat{\tau}_r = \dfrac{1}{\hat{T}_r}$, the rotor-flux estimation expression can be obtained as:

$$p\begin{bmatrix} \hat{\psi}_{r\alpha} \\ \hat{\psi}_{r\beta} \end{bmatrix} = \begin{bmatrix} -\hat{\tau}_r & -\omega_r \\ \omega_r & -\hat{\tau}_r \end{bmatrix}\begin{bmatrix} \hat{\psi}_{r\alpha} \\ \hat{\psi}_{r\beta} \end{bmatrix} + L_m\hat{\tau}_r\begin{bmatrix} i_{s\alpha} \\ i_{s\beta} \end{bmatrix} \tag{17}$$

After subtracting Equation (16) from Equation (17), the rotor-flux error is defined as:

$$pe_{\psi_r} = A_r e_{\psi_r} - w \tag{18}$$

In Equation (18), $e_{\psi_r} = \begin{bmatrix} e_{r\alpha} \\ e_{r\beta} \end{bmatrix} = \begin{bmatrix} \psi_{r\alpha} - \hat{\psi}_{ra} \\ \psi_{r\beta} - \hat{\psi}_{r\beta} \end{bmatrix}$, $A_r = \begin{bmatrix} -\tau_r & -\omega_r \\ \omega_r & -\tau_r \end{bmatrix}$, and $w = \left(\hat{\tau}_r - \tau_r\right)\left(L_m\begin{bmatrix} i_{s\alpha} \\ i_{s\beta} \end{bmatrix} - \begin{bmatrix} \hat{\psi}_{r\alpha} \\ \hat{\psi}_{r\beta} \end{bmatrix}\right)$.

For the stability analysis, ω_r and τ_r are assumed to be constant. Under these assumptions, A_r is constant, and Equation (18) can be represented by the feedback structure shown in Figure 5, with a linear time-invariant forward block and a nonlinear time-varying feedback block. When the rotor speed varies, the forward block becomes time-varying, and the transfer-function-based analysis presented here does not directly apply.

https://doi.org/10.3390/en19215289

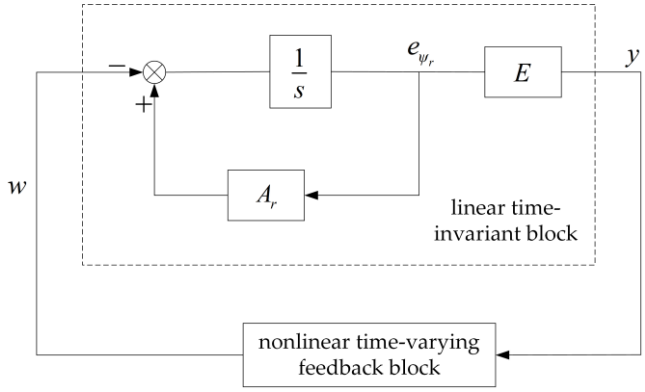


Figure 5. Standard nonlinear feedback system.

According to Popov hyperstability theory [20,21], to ensure asymptotic stability of the system, the transfer-function matrix of the linear block must satisfy the positive realness condition. Through analysis, it can be shown that the linear block satisfies the strictly positive real requirement, and the nonlinear feedback block must satisfy the Popov integral inequality, namely:

$$\eta(0,t_1)=\int_0^{t_1} y^T w dt \geq -\gamma_0^2 \tag{19}$$

In Equation (19), γ_0^2 is an arbitrary positive real number. Substituting $y=Ee_{\psi_r}=e_{\psi_r}$ and w into Equation (19) yields:

$$\eta(0,t_1)=\int_0^{t_1} e_{\psi_r}^T\left(\hat{\tau}_r-\tau_r\right)\left(L_m i_s-\hat{\psi}_r\right)dt \geq -\gamma_0^2 \tag{20}$$

In Equation (20), $e_{\psi r}^T=\begin{bmatrix} e_{r\alpha} \\ e_{r\beta} \end{bmatrix}^T=\left[e_{r\alpha}, e_{r\beta}\right]=\left[\psi_{r\alpha}-\hat{\psi}_{r\alpha}, \psi_{r\beta}-\hat{\psi}_{r\beta}\right]$.

According to the basic structure of MRAS, the estimated $\hat{\tau}_r$ is designed in the form of proportional–integral:

$$\hat{\tau}_r=\int_0^{t_1} F_1(y,\tau,t)d\tau+F_2(y,t)+\hat{\tau}_r(0) \tag{21}$$

After selecting $\hat{\tau}_r(0)$ according to the actual situation, substituting Equation (21) into Equation (20) yields:

$$\begin{aligned}\eta(0,t_1)&=\int_0^{t_1} e_{\psi_r}^T\left[\int_0^{t_1} F_1(y,\tau,t)d\tau+F_2(y,t)+\hat{\tau}_r(0)-\tau_r\right]\left(L_m i_s-\hat{\psi}_r\right)dt \\ &=\int_0^{t_1} e_{\psi_r}^T\left[\int_0^{t_1} F_1(y,\tau,t)d\tau+\hat{\tau}_r(0)-\tau_r\right]\left(L_m i_s-\hat{\psi}_r\right)dt+\int_0^{t_1} F_2(y,t)\left(L_m i_s-\hat{\psi}_r\right)dt \geq -\gamma_0^2\end{aligned} \tag{22}$$

To make (22) hold, one can take:

$$\begin{aligned}\eta_1(0,t_1)&=\int_0^{t_1} e_{\psi_r}^T\left[\int_0^{t_1} F_1(y,\tau,t)d\tau+\hat{\tau}_r(0)-\tau_r\right]\left(L_m i_s-\hat{\psi}_r\right)dt \geq -\gamma_1^2 \\ \eta_2(0,t_1)&=\int_0^{t_1} e_{\psi_r}^T\left[\int_0^{t_1} F_2(y,t)\right]\left(L_m i_s-\hat{\psi}_r\right)dt \geq -\gamma_2^2\end{aligned} \tag{23}$$

Here, γ_1 and γ_2 are positive real numbers with the same property as γ_0, so the Popov inequality can be guaranteed to hold. For convenience, let:

$$\begin{cases} K_i f(t)=\int_0^{t_1} F_1(y,\tau,t)d\tau+\hat{\tau}_r(0)-\tau_r \\ \dot{f}(t)=e_{\psi_r}^T\left(L_m i_s-\hat{\psi}_r\right) \end{cases} \tag{24}$$

From (24), we can obtain:

$$F_1(y,\tau,t) = K_i e_{\psi_r}^T \left(L_m i_s - \hat{\psi}_r\right), K_i > 0 \tag{25}$$

Then, the first term in Equation (23) satisfies:

$$\begin{aligned} \eta_1(0,t_1) &= \int_0^{t_1} K_i f(t)\dot{f}(t)dt \\ &= \frac{K_i}{2}\left[f^2(t_1) - f^2(0)\right] \geq -\frac{K_i}{2} f^2(0) \end{aligned} \tag{26}$$

Here, $\gamma_1^2 = \frac{K_i}{2} f^2(0)$. Then, Equation (26) satisfies $\eta_1(0,t_1) \geq -\gamma_1^2$.

Now, we discuss the second term in Equation (23); for convenience, let:

$$F_2(y,t) = K_p e_{\psi_r}^T \left(L_m i_s - \hat{\psi}_r\right), K_p > 0 \tag{27}$$

Then, the second term in Equation (23) satisfies:

$$\eta_2(0,t_1) = K_p \int_0^{t1} \left[e_{\psi_r}^T \left(L_m i_s - \hat{\psi}_r\right)\right]^2 dt \geq 0 \tag{28}$$

In summary, $\hat{\tau}_r$ can be designed as:

$$\hat{\tau}_r = K_p\left[e_{\psi_r}^T \left(L_m i_s - \hat{\psi}_r\right)\right] + K_i \int_0^{t_1}\left[e_{\psi_r}^T \left(L_m i_s - \hat{\psi}_r\right)\right]dt = (K_p + \frac{K_i}{s})e_\tau \tag{29}$$

In Equation (29), $i_s = \begin{bmatrix} i_{s\alpha} \\ i_{s\beta} \end{bmatrix}$, $\hat{\psi}_r = \begin{bmatrix} \hat{\psi}_{r\alpha} \\ \hat{\psi}_{r\beta} \end{bmatrix}$, $e_\tau = e_{\psi_r}^T \left(L_m i_s - \hat{\psi}_r\right)$.

Figure 6 presents the overall structure of the MRAS-based identification scheme. The rotor-flux error generated by the two models is fed into the adaptive mechanism to update $\hat{\tau}_r$ in real time and is also returned to the rotor-flux current model. The parameter convergence discussion assumes that the rotor time constant is constant during the analysis, the remaining motor parameters are accurately known, and the reference model provides the true rotor flux. Sufficient excitation of the parameter-dependent dynamics is also required to distinguish the true rotor time constant from other parameter values. Under practical conditions, reference-model errors caused by measurement offsets, parameter mismatch, and unmodelled dynamics may introduce a bias into the identified parameter. Therefore, convergence of the flux error alone is not taken as proof of exact parameter convergence. The theoretical analysis is therefore restricted to constant-speed operation with a constant rotor time constant. The simulations involving speed transients or rotor parameter changes assess the dynamic tracking performance of the method; they do not establish a general stability guarantee for time-varying operating conditions.

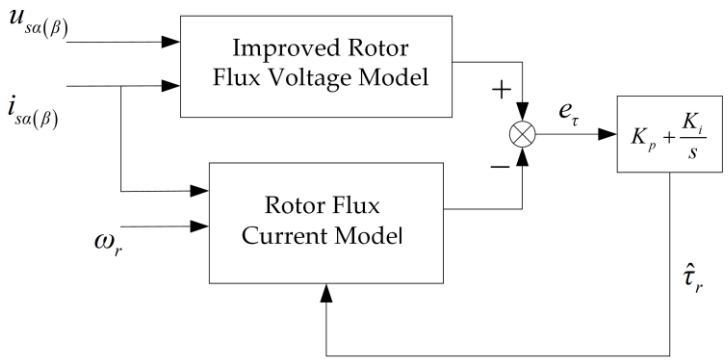


Figure 6. Rotor-flux MRAS identification system.

5. Simulation Verification

In order to examine how T_r influences indirect field-oriented control and to assess the performance of the proposed identification system, a simulation platform corresponding to Figure 7 was established in Matlab/SimulinkR2021b. The rated parameters of the induction motor employed in the tests are summarized in Table 1.

Table 1. Induction motor parameters.

Parameter	Value	Parameter	Value
Power/kW	3.7	Rotor resistance/Ω	0.8
Voltage/V	380	Mutual inductance/H	0.12
Number of pole pairs	2	Stator inductance/H	0.128
Stator resistance/Ω	0.9	Rotor inductance/H	0.128
Speed-loop proportional gain	0.35	Speed-loop integral gain	10
Current-loop proportional gain	15	Current-loop integral gain	500
Simulation time step/s	10^{-5}	Critical integral gain coefficient	10
Cutoff frequency/rad/s	100	Adaptation-law proportional gain	3
Adaptation-law integral gain	700	Initial conditions	0

From the data in the table, it can be calculated that $T_r = 0.16$ s and $\tau_r = 6.25$ s^{-1}.

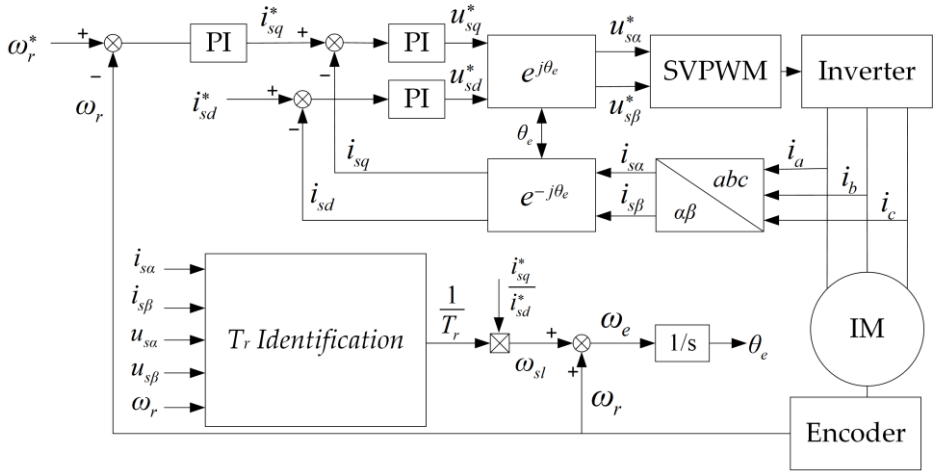


Figure 7. Induction motor vector control system.

5.1. Analysis of Simulation Results on the Effect of Tr on IFOC

The speed reference is set to 1000 r/min, and the motor starts under no-load conditions. A step load of 10 N·m is applied at 0.6 s. The actual motor rotor time constant remains at 0.16 s throughout both simulations. To examine the influence of parameter mismatch on IFOC performance, the rotor time constant used in the controller is fixed at 0.16 s in the matched case and 0.08 s in the mismatched case. All other settings remain identical. The corresponding speed and torque responses are shown in Figures 8 and 9, respectively.

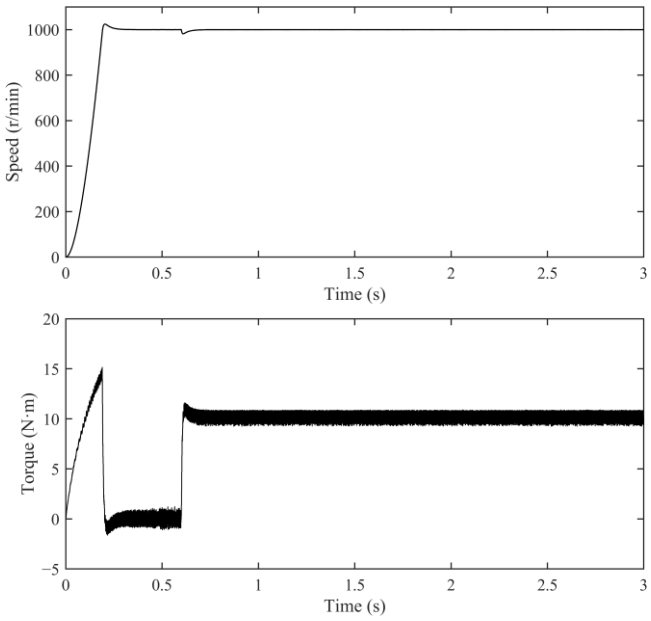


Figure 8. Speed and torque responses with a matched rotor time constant.

From Figure 8, it can be seen that when the rotor time constant used for field orientation matches the actual value, the motor speed reaches the reference at approximately 0.2 s and subsequently tracks it smoothly. When the load is applied at 0.6 s, the speed exhibits only a slight drop and quickly recovers. Figure 9 shows that a rotor time constant mismatch causes a larger speed drop and more pronounced transient oscillations in both speed and torque following load application. These oscillations gradually decay, and the speed eventually returns close to the reference. The comparison indicates that rotor time constant mismatch degrades the dynamic response to load disturbances.

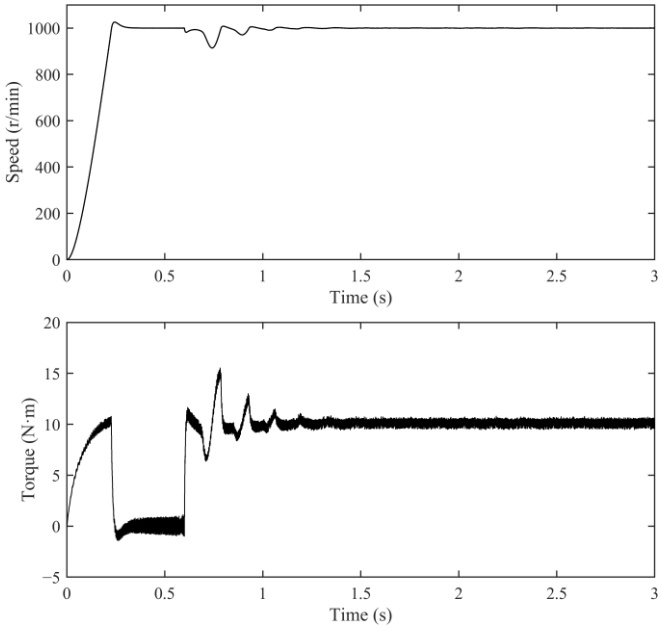


Figure 9. Speed and torque responses with a mismatched rotor time constant.

Figure 10 compares the responses with and without online updating. At 2 s, a mismatch is deliberately introduced into the rotor time constant used for field orientation. Without updating, a pronounced speed drop and transient torque oscillations occur. With updating, the MRAS estimate corrects the mismatch, keeping the speed close to its reference and substantially reducing the transient disturbance.

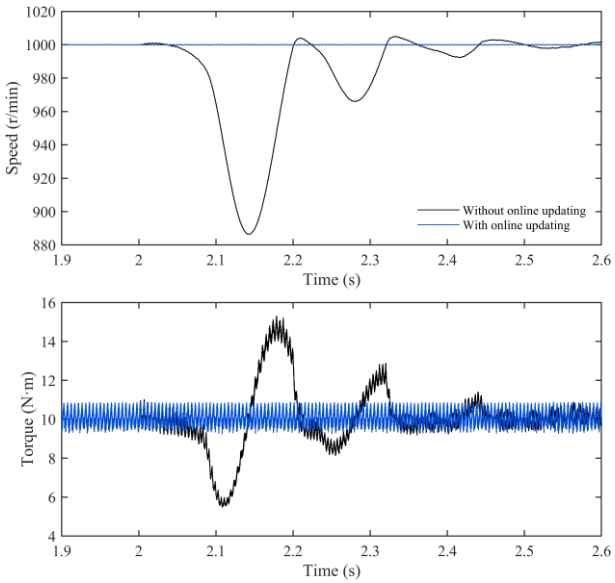


Figure 10. Speed and torque responses to an imposed controller parameter mismatch with and without online updating.

5.2. Simulation Results Analysis of the Improved Stator Flux

To evaluate the proposed stator-flux observer independently, sinusoidal back-EMF signals with an amplitude of 50 V and an angular frequency of 105 rad/s are used. At 0.3 s, DC offsets of +0.5 V and −0.5 V are introduced into the alpha- and beta-axis inputs, respectively. Figures 11 and 12 present the flux estimation results obtained using the pure integrator and the proposed observer, respectively.

The ideal flux amplitude is 0.47619 Wb. The theoretical steady-state residual flux-error vector magnitude is 0.009765 Wb, consistent with the simulation result and equivalent to 2.05% of the ideal flux amplitude. At 0.6 s, the pure-integrator error magnitude reaches 0.21213 Wb, whereas the proposed observer maintains a bounded residual error. For a quantitative comparison, the root-mean-square magnitude of the flux-error vector is evaluated over the interval from 0.5 to 0.6 s and normalized to the ideal flux amplitude. The resulting relative errors are 37.38% for the pure integrator and 2.05% for the proposed observer. These results confirm that the observer suppresses continuous integrator drift without completely eliminating the offset-induced flux error. The finite residual flux error may introduce a bias into the MRAS reference model and consequently affect the identified rotor time constant. By suppressing integrator drift, the proposed observer limits the accumulation of offset-induced reference-model errors.

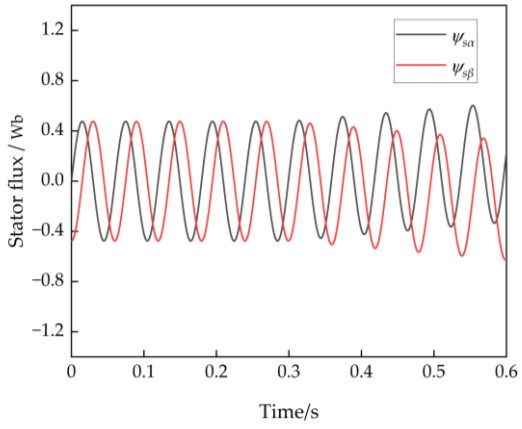


Figure 11. Stator-flux linkage observation results before improvement.

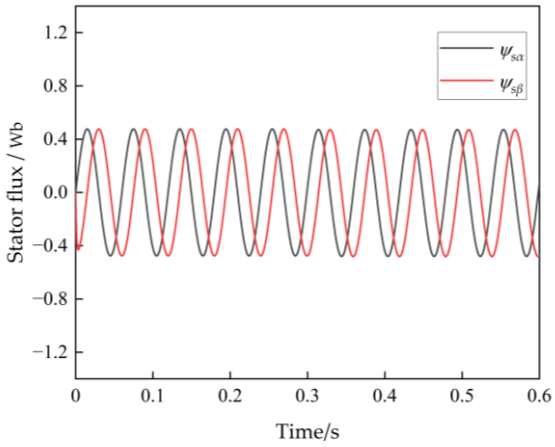


Figure 12. Stator-flux linkage observation results after improvement.

5.3. Analysis of Simulation Results of Tr Identification

Under the operating condition of a commanded motor speed of 1000 r/min with a 10 N·m load applied at 1 s, the same voltage offsets as those in Section 5.2 are used: +0.5 V and −0.5 V are introduced into the alpha- and beta-axis stator voltages, respectively, at 0.3 s. Figure 13 presents the estimated $\hat{\tau}_r$, the reciprocal of the rotor time constant, obtained with the conventional stator-flux observer when DC-offset effects are considered. The results indicate that the appearance of a DC component in the conventional stator-flux observer reduces the accuracy of the flux estimate and consequently produces an error in the identified $\hat{\tau}_r$.

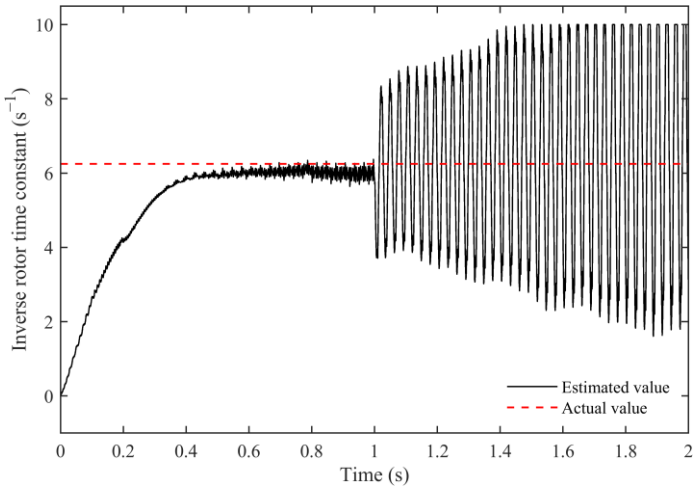


Figure 13. Estimated reciprocal of the rotor time constant obtained with the conventional stator-flux observer.

Figure 14 shows the identification result of $\hat{\tau}_r$, the reciprocal of the rotor time constant, obtained with the improved stator-flux observer. Under otherwise identical conditions, the identified value of $\hat{\tau}_r$ given by this method converges to the true value at about 0.5 s. Although a slight jitter appears in the identification result at the instant the load is applied, it quickly converges to the true value again, exhibiting better robustness than the conventional stator-flux observation method.

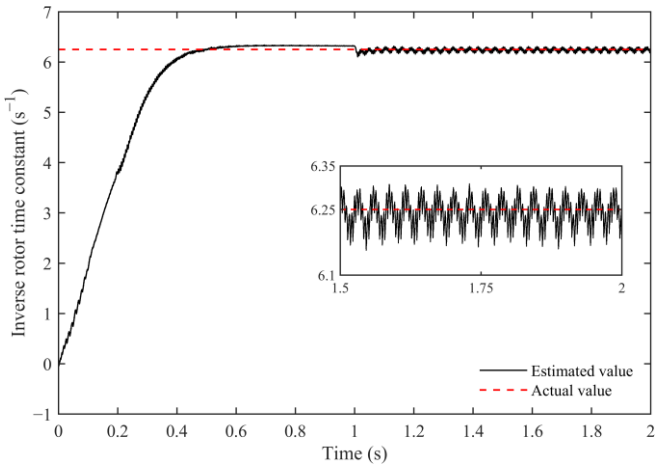


Figure 14. Estimated reciprocal of the rotor time constant.

To evaluate the dynamic tracking capability of the identification scheme, a step change in the actual motor rotor resistance is introduced at 2 s, from 0.8 Ω to 1.0 Ω, while the rotor inductance remains at 0.128 H. Consequently, the rotor time constant decreases from 0.16 s to 0.128 s, and its reciprocal increases from 6.25 s^{-1} to 7.8125 s^{-1}. The corresponding identification response is shown in Figure 15.

Rotor resistance can vary with operating conditions, particularly rotor temperature. However, the instantaneous resistance step used here is an idealized parameter perturbation intended to assess the response of the identification scheme to a known change. It does not reproduce the gradual thermal evolution of rotor resistance or the coupled parameter variations associated with magnetic saturation. The result therefore demonstrates parameter-tracking performance under the specified step-change condition.

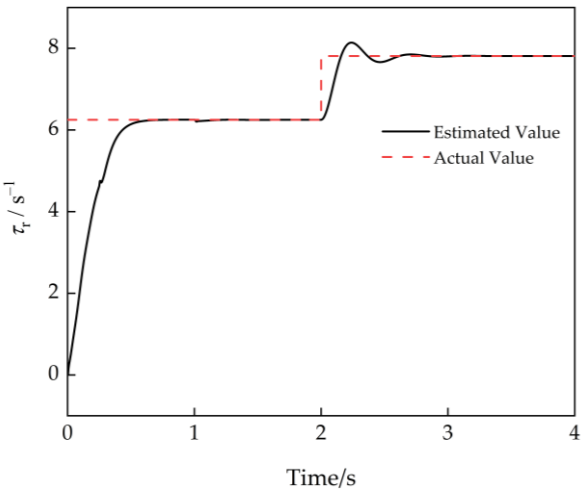


Figure 15. Identification results under rotor time constant sudden change.

To further assess the identification performance under a discrete implementation, an additional test is conducted with a speed reference of 1000 r/min and a 10 N·m load applied at 0.8 s. The controller and identification update period is 100 μs, corresponding to 10 kHz, while the power-system discrete sample time is 10 μs. The voltage and current inputs to the identification scheme are averaged over the preceding PWM period. The adjustable rotor-flux current model uses an exact zero-order-hold state transition, with its inputs and parameters held constant within each update interval. The identification response is shown in Figure 16. The estimate approaches the actual inverse rotor time constant and exhibits a small residual bias and ripple. Over the interval from 2.5 s to 3 s, the

mean estimate is 6.3394 s^{-1}, compared with the actual value of 6.25 s^{-1}. The relative mean bias and relative root-mean-square error are 1.43% and 1.47%, respectively. These results demonstrate identification performance under the specified discrete implementation.

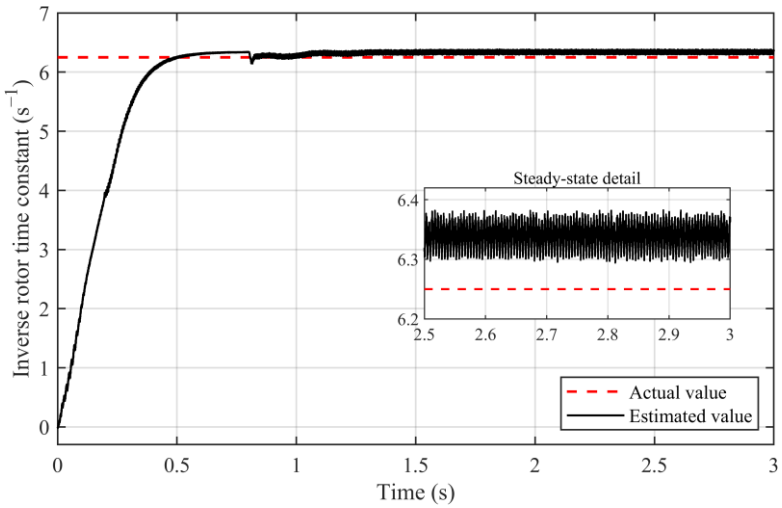


Figure 16. Inverse rotor time constant estimation with a discrete implementation.

To further evaluate the identification scheme with a discrete implementation and inverter dead time, additional simulations are performed with a control and identification update period of 100 microseconds and an electrical simulation time step of 1 microsecond. The speed reference is set to 1000 r/min, and a load torque of 10 N·m is applied at 0.8 s. The measured voltage and current signals are averaged over each PWM period before being supplied to the identification scheme. The adjustable rotor-flux model is implemented using an exact state transition with its inputs and estimated parameters held constant over each update interval. Two cases are compared under otherwise identical conditions: without dead time and with a dead time of 2 microseconds. As shown in Figure 17, both estimates converge close to the actual inverse rotor time constant of 6.25 s−1 and recover following the load application. Over the interval from 2.5 to 3 s, the mean estimated values are 6.2813 s−1 without dead time and 6.2854 s−1 with dead time, corresponding to relative mean biases of 0.50% and 0.57%, respectively. The corresponding relative root-mean-square errors are 0.50% and 0.57%. Although dead time slightly increases the estimation bias and ripple, its influence remains limited under the tested operating conditions.

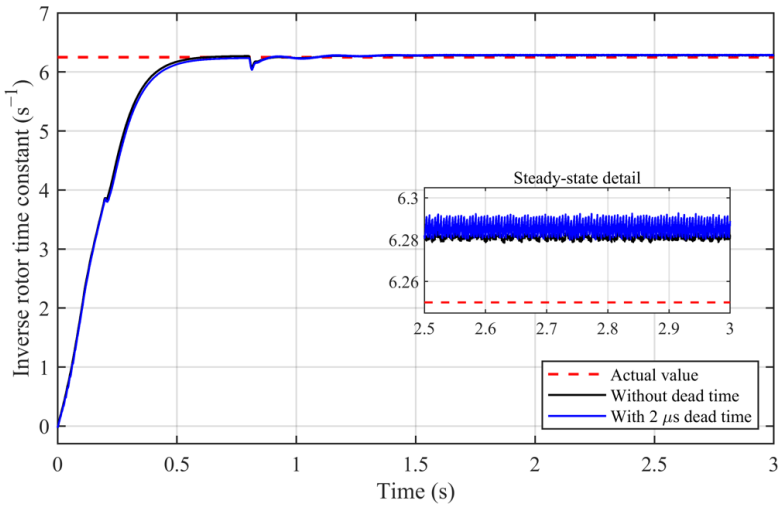


Figure 17. Inverse rotor time constant estimation with and without inverter dead time.

To examine the sensitivity of the identification scheme to stator resistance mismatch at low speed, an additional test is conducted with a speed reference of 100 r/min. The actual motor stator resistance is set to 0.5 Ω, whereas the reference model retains the nominal value of 0.9 Ω. As shown in Figure 18, the estimated inverse rotor time constant deviates substantially from the actual value of 6.25 s^{-1}. Although the oscillations in the later part of the response decrease, a considerable estimation bias remains over the simulated interval. This result illustrates a limitation of the voltage-model-based reference flux under the combined conditions of low-speed operation and stator resistance mismatch. At low synchronous electrical frequencies, the reduced back electromotive force increases the relative influence of inaccuracies in the stator resistance drop. The resulting reference-flux error may be partially compensated by an adjustment of the estimated rotor time constant, introducing identification bias. Although the proposed feedback compensation suppresses integrator drift, it does not eliminate errors caused by stator resistance mismatch. Accurate stator resistance information or appropriate compensation is therefore important, particularly at low synchronous frequencies.

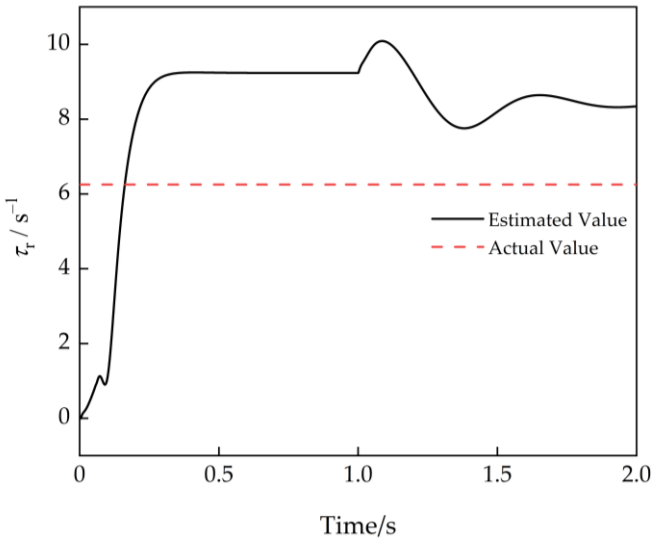


Figure 18. Inverse rotor time constant estimation under low-speed operation and stator resistance mismatch.

6. Conclusions

To overcome the field-orientation error induced by rotor time-constant drift under indirect field-oriented control of induction motors, an online identification approach that relies on an improved stator-flux model is presented. A DC-offset compensation mechanism is introduced, thereby raising the accuracy of the stator-flux estimate. On this basis, an MRAS framework is established for identifying the rotor time constant. Under the specified DC-offset condition, the proposed observer reduces the relative flux estimation RMSE from 37.38% to 2.05%. The inverse rotor time constant estimate enters a ±2% error band in approximately 0.43 s before load application, with a relative root-mean-square error of 0.51% over the interval from 1.5 to 2 s. These results demonstrate improved flux estimation and parameter identification under the tested conditions. Nevertheless, a finite residual flux error remains, and the low-speed test with stator resistance mismatch reveals sensitivity to reference-model inaccuracies. Future work will address these limitations and include experimental validation.

Author Contributions: Conceptualization, H.H. and Y.Z.; methodology, H.H.; software, H.H.; validation, H.H.; formal analysis, H.H.; investigation, H.H.; data curation, H.H.; writing—original

draft preparation, H.H.; writing—review and editing, Y.Z.; visualization, H.H. All authors have read and agreed to the published version of the manuscript.

Funding: This research received no external funding.

Data Availability Statement: All data generated or analyzed during this study are included in this published article.

Conflicts of Interest: The authors declare no conflicts of interest.

Nomenclature

ω_{sl}	Slip electrical angular frequency
ω_r	Rotor electrical angular frequency
ω_e	Synchronous electrical angular velocity
i_{sd}	d-axis stator current
i_{sq}	q-axis stator current
T_r	Rotor time constant
L_r	Rotor inductance
R_r	Rotor resistance
θ_e	Rotor field phase angle
θ_r	Rotor position angle
θ_{sl}	Slip angle
$\psi_{s\alpha}$	α -axis stator flux
$\psi_{s\beta}$	β -axis stator flux
$u_{s\alpha}$	α -axis stator voltage
$u_{s\beta}$	β -axis stator voltage
$i_{s\alpha}$	α -axis stator current
$i_{s\beta}$	β -axis stator current
$\psi_{r\alpha}$	α -axis rotor flux
$\psi_{r\beta}$	β -axis rotor flux
L_m	Mutual inductance
σ	Leakage coefficient
$u_{r\alpha}$	α -axis rotor voltage
$u_{r\beta}$	β -axis rotor voltage
$i_{r\alpha}$	α -axis rotor current
$i_{r\beta}$	β -axis rotor current
R_s	Stator resistance
p	Differential operator
T_e	Electromagnetic torque
n_p	The number of pole pairs
e_s	Stator back electromotive force
ψ_s	Stator-flux linkage
Δd	DC component
ψ_s^v	Improved stator flux
K_λ	Compensation feedback gain
ω_c	Cutoff frequency
C	Critical integral gain coefficient
τ_r	Reciprocal of the rotor time constant
e_{ψ_r}	Rotor-flux error

i_s	Stator current
ψ_r	Rotor-flux linkage
K_p	Proportional coefficient
K_i	Integral coefficient

References

1. Nagataki, M.; Kondo, K.; Yamazaki, O.; Yuki, K. First-Order-Delay-Controlled Slip-Angular Frequency for the Dynamic Performance of an Indirect-Field-Orientation-Controlled Induction Motor-Driving Inertial Load. *IEEE Open J. Ind. Appl.* **2023**, *4*, 160–177. https://doi.org/10.1109/OJIA.2023.3275645.
2. Cao, P.P.; Zhang, X.; Yang, S. A Unified-Model-Based Analysis of MRAS for Online Rotor Time Constant Estimation in an Induction Motor Drive. *IEEE Trans. Ind. Electron.* **2017**, *64*, 4361–4371. https://doi.org/10.1109/TIE.2017.2668995.
3. Zhang, J.; Zhang, X.; Yu, Y.; Wang, B.; Xu, D.G. A model reference adaptive system-based online rotor time constant estimation method for induction motor field-weakening control utilizing dot product of stator voltage and stator current. *IEEE Trans. Transp. Electrif.* **2024**, *10*, 3576–3589. https://doi.org/10.1109/TTE.2023.3310517.
4. Azab, M. A Review of Recent Trends in High-Efficiency Induction Motor Drives. *Vehicles* **2025**, *7*, 15. https://doi.org/10.3390/vehicles7010015.
5. Konuhova, M. Modeling of Induction Motor Response to Voltage Sags with Re-Acceleration Analysis. *Energies* **2025**, *18*, 5682. https://doi.org/10.3390/en18215682.
6. Tang, J.; Yang, Y.; Blaabjerg, F.; Chen, J.; Diao, L.; Liu, Z. Parameter Identification of Inverter-Fed Induction Motors: A Review. *Energies* **2018**, *11*, 2194. https://doi.org/10.3390/en11092194.
7. Xiong, Z.W. A rotor time constant on-line identification method for induction motor. *Mach. Tool. Hydraul.* **2019**, *47*, 149–153. https://doi.org/10.3969/j.issn.1001-3881.2019.04.035.
8. Zhang, X.X.; Wang, Q.W.; Wang, G.L.; Zhang, G.Q.; Xu, D.G. Review of parameter identification techniques for induction motors. *J. Electr. Eng.* **2025**, *20*, 43–60. https://doi.org/10.11985/2025.04.003.
9. Chen, D.D.; Kong, W.B.; Qu, R.H.; Zhou, L.B. Correction of field orientation inaccuracy caused by resolver periodic error and rotor time constant variation for indirect field-oriented control induction motor drives. *IEEE Trans. Ind. Electron.* **2022**, *69*, 4440–4450. https://doi.org/10.1109/TIE.2021.3078402.
10. Cao, P.P.; Zhang, X.; Yang, S.Y.; Xie, Z.; Guo, L.L. Online rotor time constant identification of induction motors based on Lyapunov stability theory. *Proc. CSEE* **2016**, *36*, 3947–3955. https://doi.org/10.13334/j.0258-8013.pcsee.151564.
11. Yang, S.Y.; Ding, D.W.; Li, X.; Xie, Z.; Zhang, X.; Chang, L.C. A novel online parameter estimation method for indirect field oriented induction motor drives. *IEEE Trans. Energy Convers.* **2017**, *32*, 1562–1573. https://doi.org/10.1109/TEC.2017.2699681.
12. Ray, N.K.; Das, S.; Goswami, G. Active power based MRAS for estimation of inverse rotor time constant in field-oriented control of induction motor drive. *IEEE Trans. Ind. Appl.* **2026**, *62*, 2687–2699. https://doi.org/10.1109/TIA.2025.3605306.
13. Zerdali, E. A comparative study on adaptive EKF observers for state and parameter estimation of induction motor. *IEEE Trans. Energy Convers.* **2020**, *35*, 1443–1452. https://doi.org/10.1109/TEC.2020.2979850.
14. Han, Y.; Kim, H.; Lee, K. Dual MRAS for robust rotor time constant compensation in IFOC IM drives. *IEEE Trans. Energy Convers.* **2024**, *39*, 1983–1993. https://doi.org/10.1109/TEC.2024.3361453.
15. Zhang, X.; Zhang, Y.W.; Yang, S.Y.; Cao, P.P.; Xie, Z. An improved MRAS for rotor time constant updating in induction motor drives utilizing dot product of stator current and rotor flux. *IEEE Trans. Power Electron.* **2019**, *34*, 8905–8915. https://doi.org/10.1109/TPEL.2018.2884344.
16. Zhong, Y.; Shen, Y.; Wang, H.; Zhao, C.; Lee, C.H.T. A Novel ROGI-PNSS Flux Observer Based Sensorless Control for PMSM Considering Negative-Sequence Disturbance. *IEEE Trans. Ind. Electron.* **2026**, *73*, 14262–14274. https://doi.org/10.1109/TIE.2026.3684196.
17. Weng, Z.W.; Cui, Y.L.; Zhou, Z.J. Speed sensorless model reference adaptive control for induction motors. *Mach. Tool. Hydraul.* **2024**, *52*, 7. https://doi.org/10.3969/j.issn.1001-3881.2024.18.001.
18. Saleh, A.A.; Hassan, M.A.; Said, T.M.; Adel, M.M. A Predictive Finite Speed-Set MRAS for Robust Sensorless Control of PMSM Drives in Electric Vehicles Under Driving Cycle. *Machines* **2026**, *14*, 788.
19. Zaky, M.S.; Metwaly, M.K. Improved MRAS observer with rotor flux correction terms and FLC-based adaptive law for sensorless induction motor drives. *Sci. Rep.* **2025**, *15*, 14769. https://doi.org/10.1038/s41598-025-98178-7.

20. Zhao, H.S.; Du, Z.L.; Liu, X.F.; Wang, Q. An On-line Identification Method for Rotor Resistance of Squirrel Cage Induction Motors Based on Recursive Least Square Method and Model Reference Adaptive System. *Proc. CSEE* **2014**, *34*, 5386–5394. https://doi.org/10.13334/j.0258-8013.pcsee.2014.30.016.
21. Tir, Z.; Orowska-Kowalska, T.; Ahmed, H.; Houari, A. Adaptive High Gain Observer Based MRAS for Sensorless Induction Motor Drives. *IEEE Trans. Ind. Electron.* **2023**, *71*, 271–281. https://doi.org/10.1109/TIE.2023.3243271.

Disclaimer/Publisher's Note: The statements, opinions and data contained in all publications are solely those of the individual author(s) and contributor(s) and not of MDPI and/or the editor(s). MDPI and/or the editor(s) disclaim responsibility for any injury to people or property resulting from any ideas, methods, instructions or products referred to in the content.